The submitted manuscript has been authore
by a contractor of the U. S. Governme
under contract No. W-31-109-ENG-3
Accordingly, the U. S. Government retains
nonexclusive, royalty-free license to publi
or reproduce the published form of th
contribution, or allow others to do so, f
U. S. Government purposes.

LS-155
W. Chou
Jan 20, 1989
(Rev. September 4, 1990)

3-D Computer Simulations of EM Fields in the APS Vacuum Chamber — Part 2: Time-Domain Analysis

In Ref. [1], we analyze the RF modes of the 1-meter-long sector of the APS vacuum chamber in the frequency-domain. This note is a parallel analysis in the time-domain.

There are quite a few measurements completed on this 1-meter-long sector. [2] In order to understand these experimental results, in particular, the cause of the strong peak around 4 GHz observed in the narrow gap, the 3-D real-time computer simulations are carried out using MAFIA. [3] In these simulations, the vacuum chamber is approximated by the geometry shown in Fig. 1. The 1-inch-diameter beampipes, which are attached at both ends of the beam chamber, are infinitely long (so-called the open boundary condition). A Gaussian-distributed rigid bunch traverses this structure along (or slightly above) the axis of the beampipes and generates wakefields, which are computed by the time-domain solver T3. Five probes are placed inside the top of the vacuum chamber along the horizontal direction. One is in the beam chamber, three in the narrow gap and one in the antechamber, see Fig. 1(b). These probes record the **E** and **H** fields at each location as a function of the wall clock time t. The $\mathbf{E}(t)$ and $\mathbf{H}(t)$ are then Fourier-transformed and the spectra are compared with that obtained from measurements.

The resolution of our Fourier transform is about 0.17 GHz. This means that there are about 60 points in the region from 0 to 10 GHz, within which the real and imaginary parts of the Fourier transform of $\mathbf{E}(t)$ and $\mathbf{H}(t)$ are plotted. The power spectra, which are the sum of the squares of the two parts, is not plotted; but its peaks should be easily located in the figures below.

Several types of simulations have been performed, each using the upper half of the geometry but with different configurations and boundary conditions.

1. The sector is 1-m-long. The bunch has an r.m.s. length, σ_b, of 2 cm (67 ps). The $y = 0$ plane is a magnetic boundary (permeability $\mu = \infty$). The 1-inch-diameter beam holes are at the center of the beam chamber.

2. Same as 1, but the beam holes are displaced horizontally by 1 cm.

3. The sector is 10-cm-long. The bunch length, σ_b, is 0.75 cm (25 ps). The $y = 0$ plane is a metallic boundary (conductivity $\sigma = \infty$). The beam holes are at the center of the beam chamber.

4. Same as 3, but the beam holes are displaced horizontally by 1 cm.

The main results of these runs are shown in Figs. 2-5, and are explained below.

1. In run 1, the boundary conditions at the $y = 0$ plane allow for TM_{m1} modes [1] but eliminate TE_{m0} modes in the narrow gap [2]. The cutoff frequency of the TM waves, i.e., the frequency of TM_{11} mode, of the gap is about 15 GHz and is much higher than that of the beam chamber, which is about 4.6 GHz (see [4]). Therefore, we do not see any significant field components in the gap, nor in the antechamber. As shown in Figs. 2(a)-(c), the **E** fields in the beam chamber have a magnitude of 10^{13} V/m, while that in the gap and in the antechamber are, respectively, five and ten orders of magnitude lower. In other words, the TM modes do not couple between the beam chamber and the antechamber, as expected.

   Figs. 2(d) and (e) show the spectra of the **E** fields at probe 1 in the beam chamber. It is seen that the spectrum of E_y contains low-frequency componenets, which are TE modes, whereas that of E_z starts at about 4.6 GHz, consistent with the excitation of the first TM mode.

2. The results of run 2 are similar to that of run 1.

3. In run 3, the boundary conditions at the $y = 0$ plane do allow for TE_{m0} modes in the gap. The cutoff of TE_{m0} is low (about 0.33 GHz [2]). When the bunch enters the beampipe, TM waves are generated and propagate. These TM waves get scattered at the discontinuous corner between the beam holes and the beam chamber. The scattering excites TE waves, which can then easily penetrate into the gap as well as into the antechamber.

   To convince oneself that this is a correct picture, let us compare the time delay of the starting point, the first peak and the first big peak of the E_y field observed at Probes 1, 3 and 5, with that calculated from the geometry. The calculations are demonstrated in Fig. 3, in which the time needed for electromagnetic waves propagating from one point to another is indicated in nanoseconds. The r.m.s. bunch length, σ_b, is 0.025 ns. Half of the total bunch length is 5 σ_b, namely, 0.125 ns, which has to be taken into account. Let us now take Probe 3 as an example to demonstrate our calculations. The distance between the entrance and Probe 3 is 0.47 ns. This is when the E-field starts to show up at Probe 3. As the bunch center enters this geometry, which gives another time delay of 0.125 ns (5 σ_b), we see the first peak of E_y. When the bunch center reaches the discontinuous corner between the exit beam hole and the beam chamber, the back-scattered waves will enhance the fields at Probe 3 so that we will see a big peak as shown in Fig. 4(c). The total time delay for this big peak is 0.8 ns (Fig. 3) plus 0.125 ns, i.e., 0.925 ns. Table 1 gives a complete list of the results of this comparison. The good agreement between the observation and the calculation supports the explanation given in the previous paragraph.

[1] Here the notations of rectangular waveguides are adopted, namely, the subscripts of $TM(TE)_{m,n}$ stand for the number of half-waves in the x, y direction, respectively.

[2] The TE_{0n} modes are also allowed for in the gap. But we have no interest in them, because their high cutoff frequency prevents them from penetrating into the gap.

Furthermore, our results also indicate that the fields penetrating into the gap and the antechamber are TE waves. Fig. 4 shows that the major E component, E_y, has about the same magnitude of 10^{13} V/m across the whole vacuum chamber — in the beam chamber, in the gap and in the antechamber. The E_z component is negligible (five to seven orders of magnitude lower than that of E_y) in the gap as well as in the antechamber. On the other hand, the H_z and H_x components of the magnetic fields across the vacuum chamber have about the same magnitude (10^{10} A/m), and the H_y in the gap is insignificant (seven orders of magnitude lower). Therefore, we claim that the modes in the gap are of the TE type.

Because the cutoff of TM modes in the beam chamber is about 4.6 GHz, it is conceivable that the TE wave spectra will have its first peak around this frequency. This is justified by Fig. 4(d), which shows that the first peak of E_y in the gap is indeed close to 4.6 GHz. The measured frequency of this peak is about 4 GHz, which is somewhat lower than our simulation results. One possible explanation for this discrepency is that the resolution of the measured spectra is relatively rough (about 0.5 GHz). One may, of course, equally well argue that the results of MAFIA output are not accurate enough.

The fields at probes 2, 3 and 4 in the gap and that at probe 5 in the antechamber are all of the same magnitudes. This is in contrast with the measurements, which show that the fields at probes 2, 4 and 5 are much weaker than that at probe 3. The reason is unknown.

4. In run 4, when the beam holes are displaced along the horizontal axis, the fields at probe 3 remain about the same as that in run 3, as can be seen in Fig. 5. This is again in contrast with the measurements, which show that, in this case, the fields in the gap are greatly suppressed.

In summary, our simulations suggest that the strong peak around 4 GHz in the narrow gap observed in the measurements is generated by TE modes. Therefore, one should not worry about this peak insofar as the coupling impedance is concerned. (Recall that TE waves do not contribute to the impedance.) On the other hand, some discrepencies between our simulations and the measurements are noticed and remain to be resolved.

The author thanks Dr. T. Khoe and Dr. J. Cook for their helpful discussions.

Table 1. Time Delay -- Comparison between Observation and Calculation

	Probe 1		Probe 3		Probe 5	
	(o)	(c)	(o)	(c)	(o)	(c)
Starting pt. (ns)	0.23	0.23	0.47	0.47	0.8	0.81
1st peak (ns)	0.36	0.355	0.6	0.595	0.93	0.935
1st big peak (ns)	(ditto)		0.9	0.925	N/A	N/A

Notes: (o) observation [see Fig. 4(a), (c) and (e)].
(c) calculation [see Fig. 3].

References

[1] W. Chou and J. Bridges, *3-D Computer Simulations of EM Fields in the APS Vacuum Chamber — Part 1: Frequency-Domain Analysis*, ANL Light Source Note LS- (1990).
157

[2] R. Kustom, J. Bridges, W. Chou, J. Cook, G. Mavrogenes and G. Nicholls, *Analysis of RF modes in the ANL APS Vacuum Chamber Using Computer Simulation, Electron Beam Exitation, and Perturbation Techniques*, 1989 Particle Accelerator Conference, Chicago, Illinois, March 20-23, 1989.

[3] T. Weiland, IEEE Trans. Nucl. Sci., NS-32, 2738 (1985).

[4] W. Chou and Y. Jin, *Impedance Studies - Part 4: The APS Impedance Budget*, ANL Light Source Note LS-115 (1988).

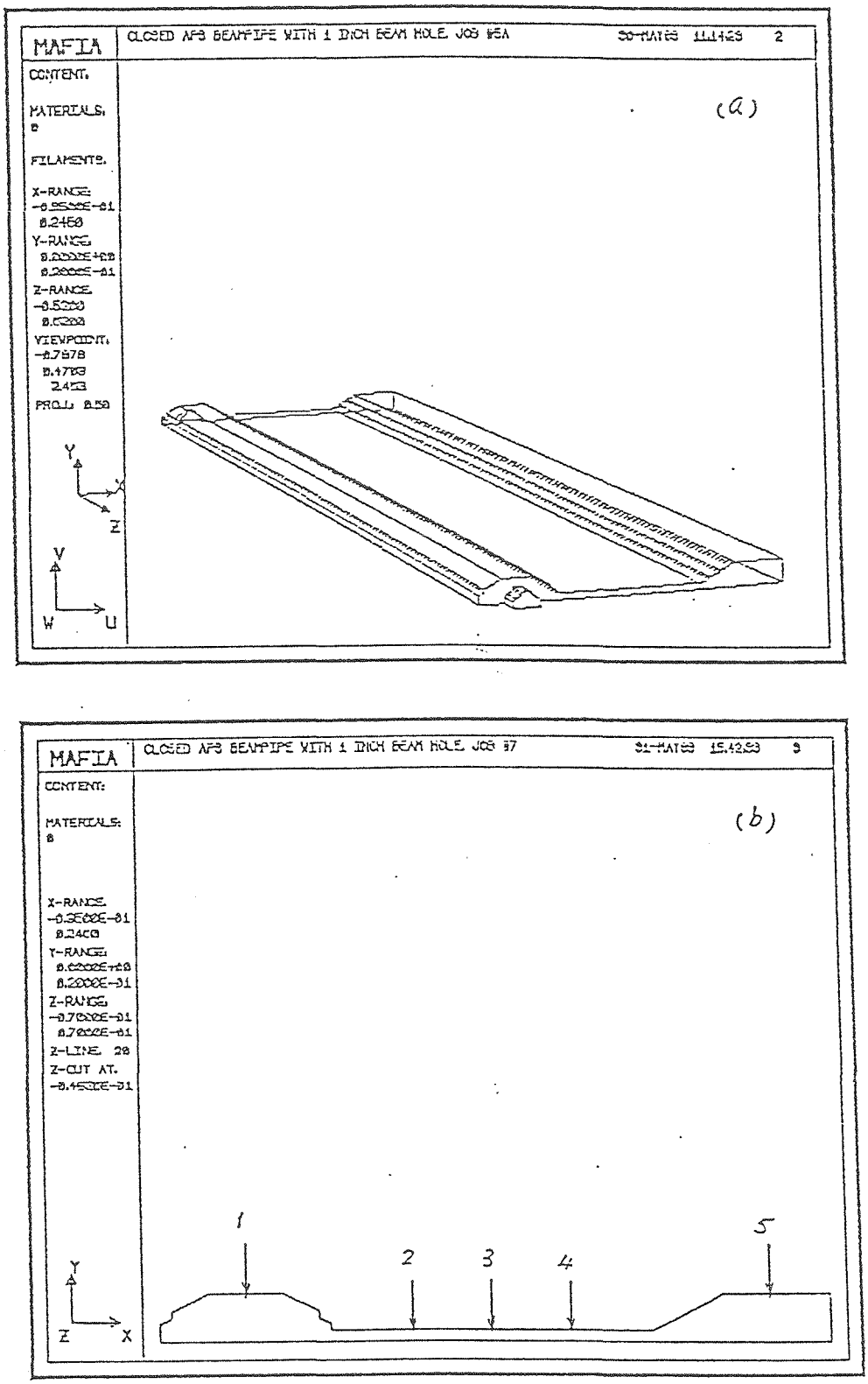

Fig. 1. (a) The geometry used in the 3-D simulations. The 1-inch- diameter beampipes are infinitely long. (b) The cross-section of the vacuum chamber in the x-y plane and the locations of five probes.

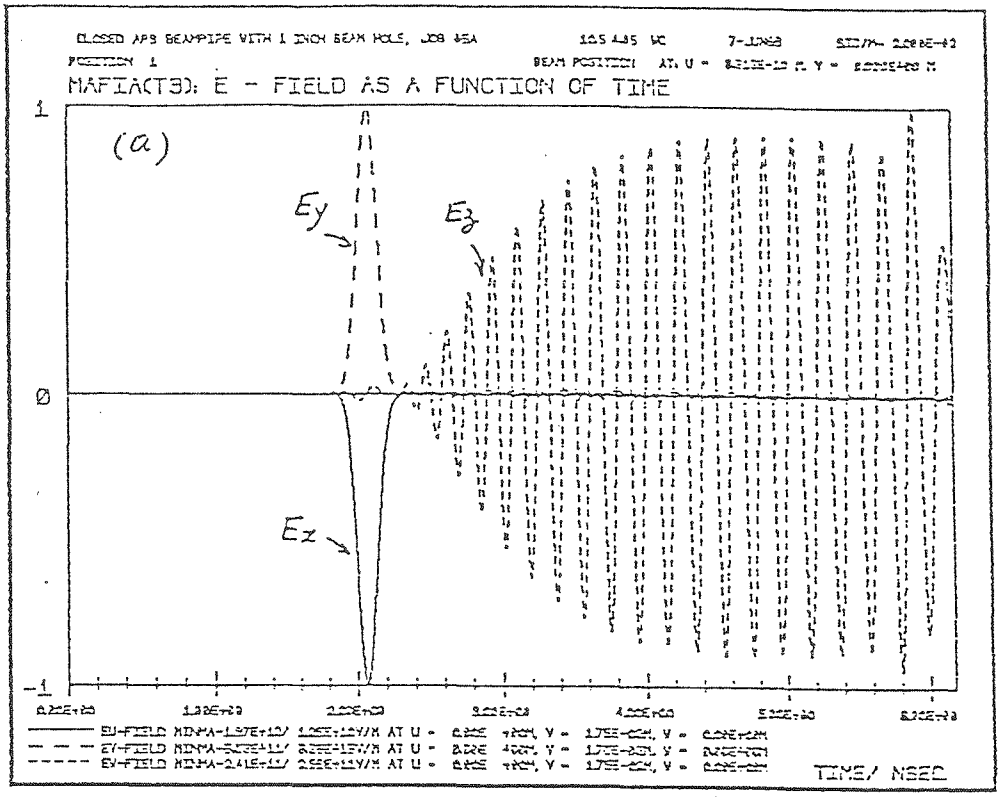

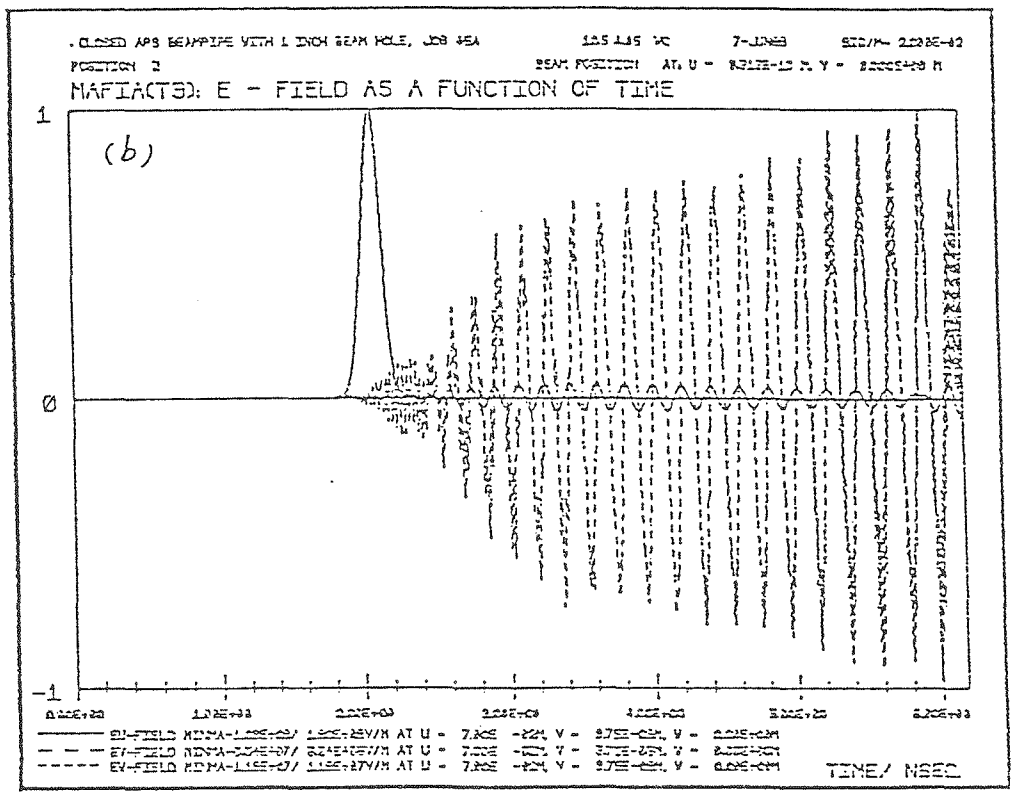

Fig. 2. The $\mathbf{E}(t)$ fields and their spectra obtained from run 1 (see text).
(a) $\mathbf{E}(t)$ fields in the beam chamber, with magnitude 10^{13} V/m.
(b) $\mathbf{E}(t)$ fields in the narrow gap, with magnitude 10^{8} V/m.

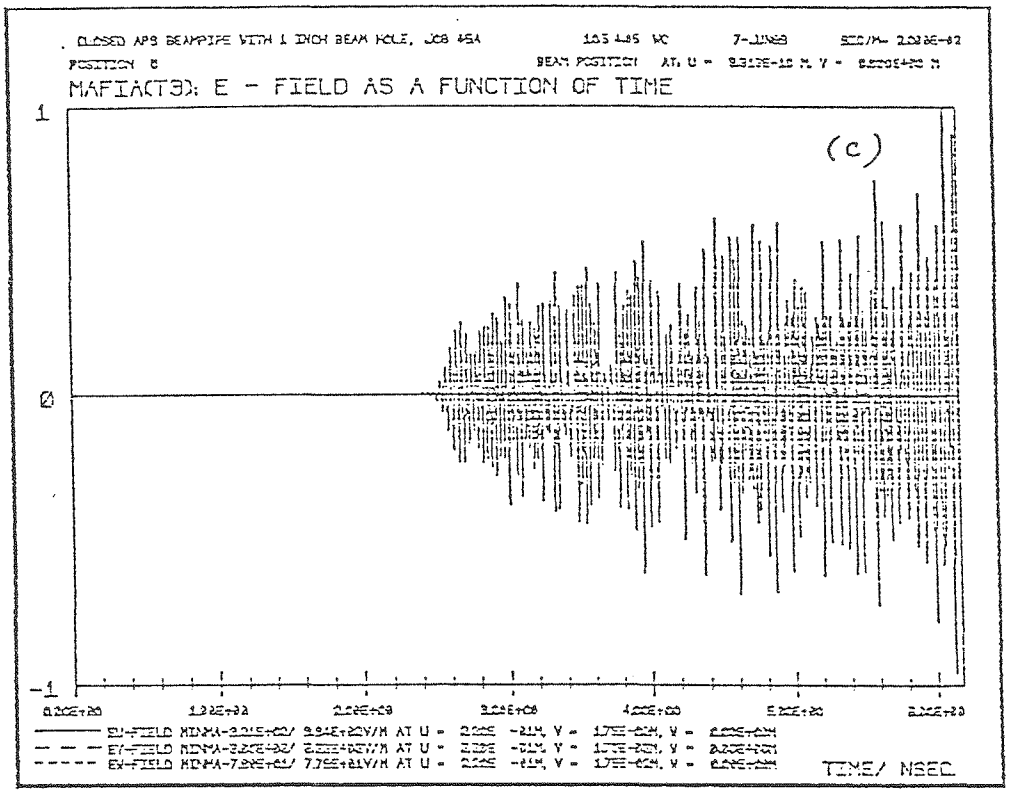

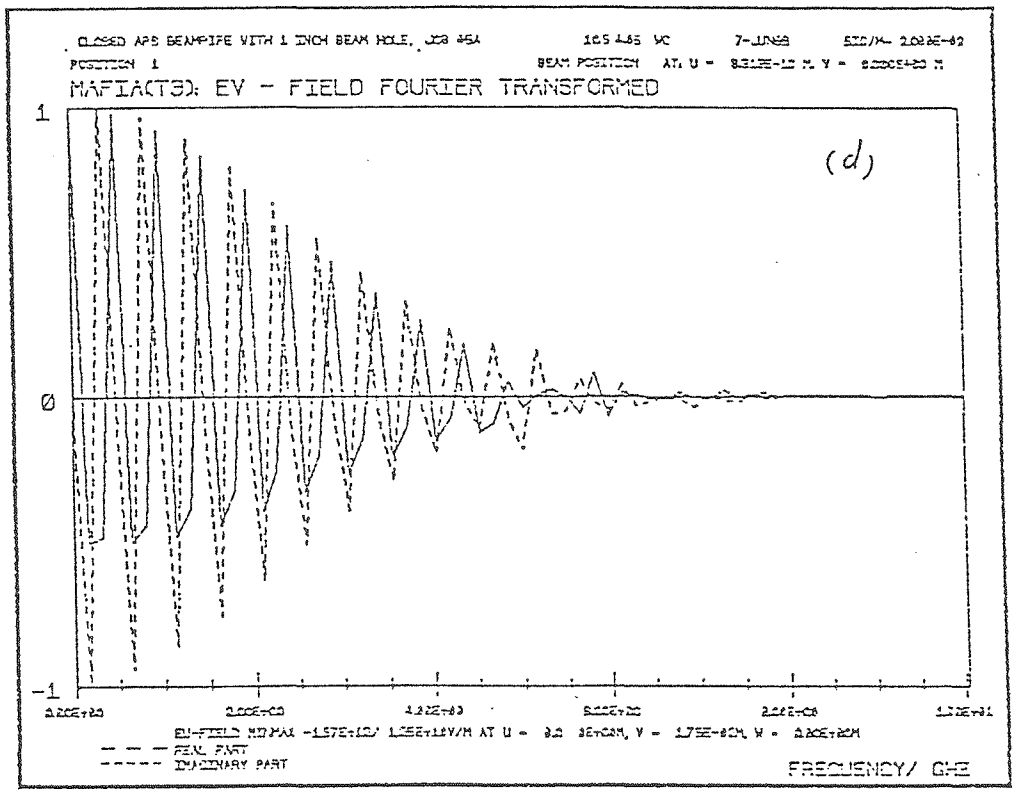

Fig. 2. (c) E(t) fields in the antechamber, with magnitude 10^2 V/m.
(d) The spectrum of the Fourier transform of E_y in the beam chamber.

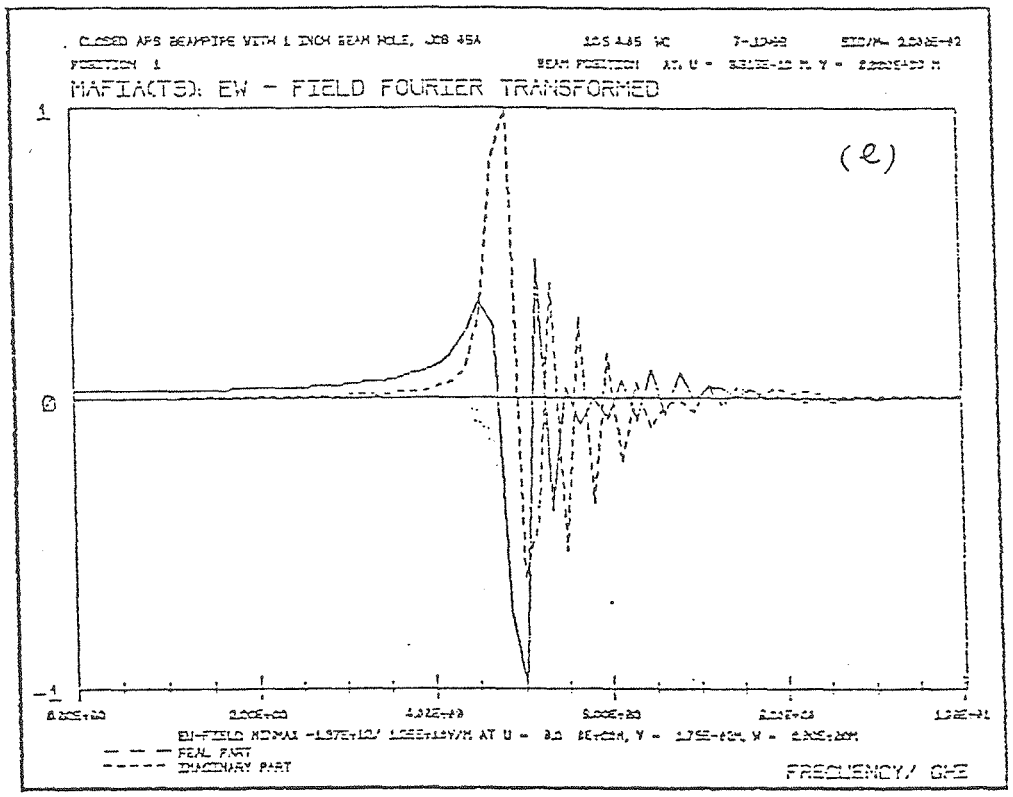

Fig. 2. (e) The spectrum of the Fourier transform of E_z in the beam chamber.

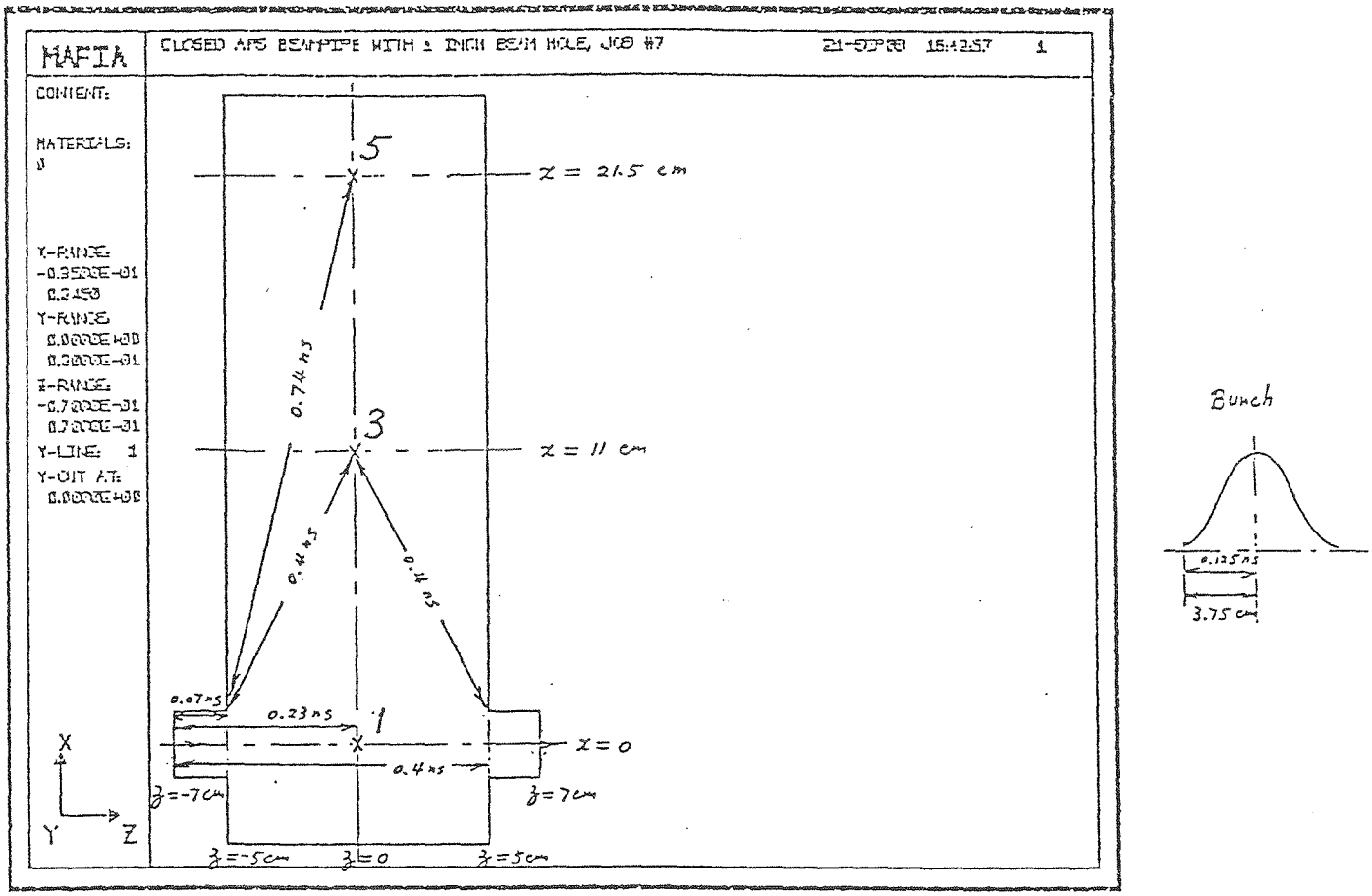

Fig. 3. This is the cross-section of the vacuum chamber in the x-z plane. 1, 3 and 5 are the locations of three probes. The distance between two points is indicated in nanoseconds. The distance between the bunch head and the bunch center is also indicated.

(a)

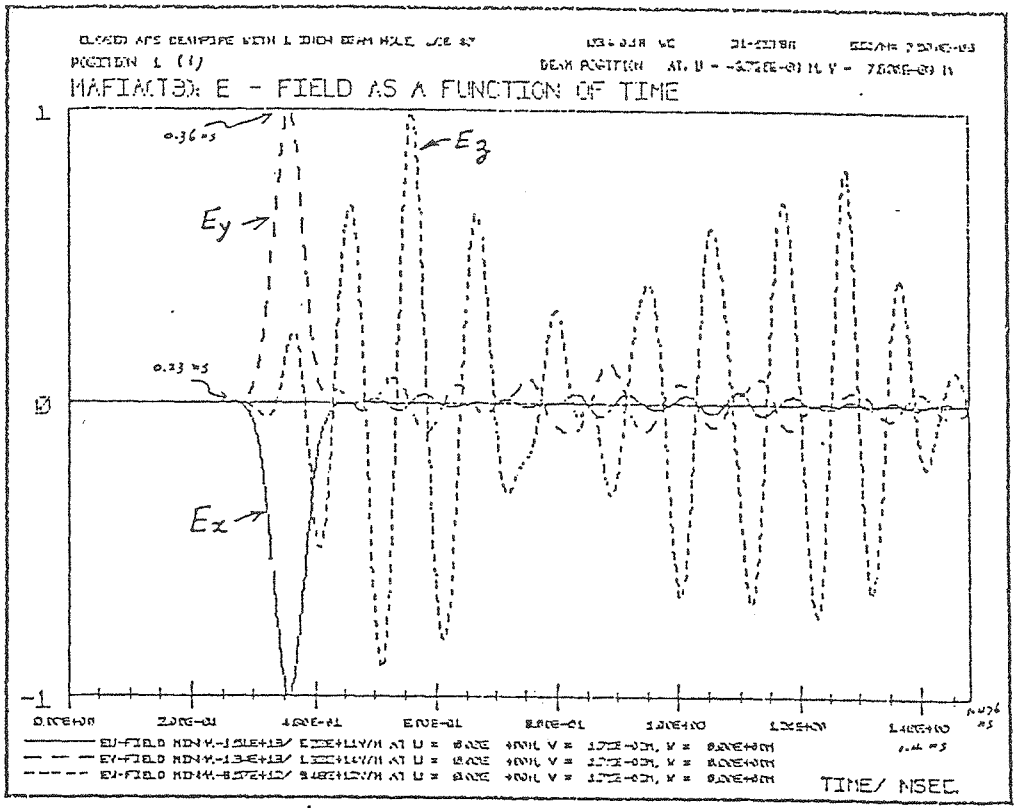

(b)

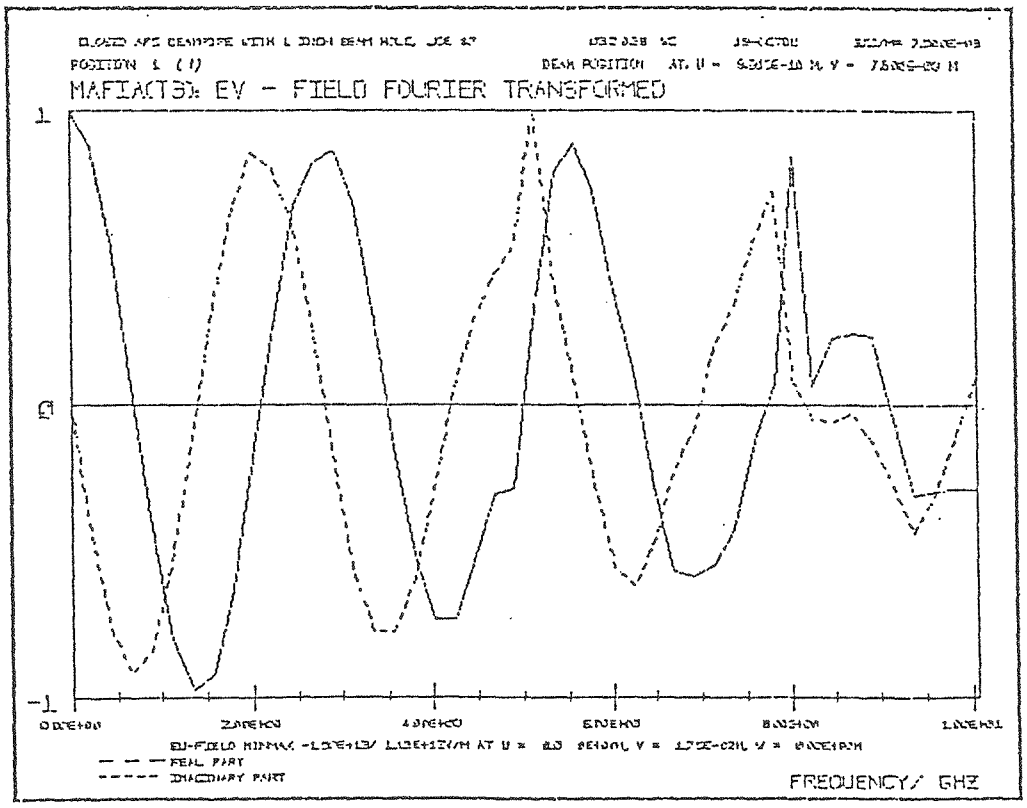

Fig. 4. The E(t) fields and their spectra obtained from run 3 (see text).
(a) E(t) fields in the beam chamber, with magnitude 10^{13} V/m.
(b) The Fourier transform of E_y in the beam chamber.

(c)

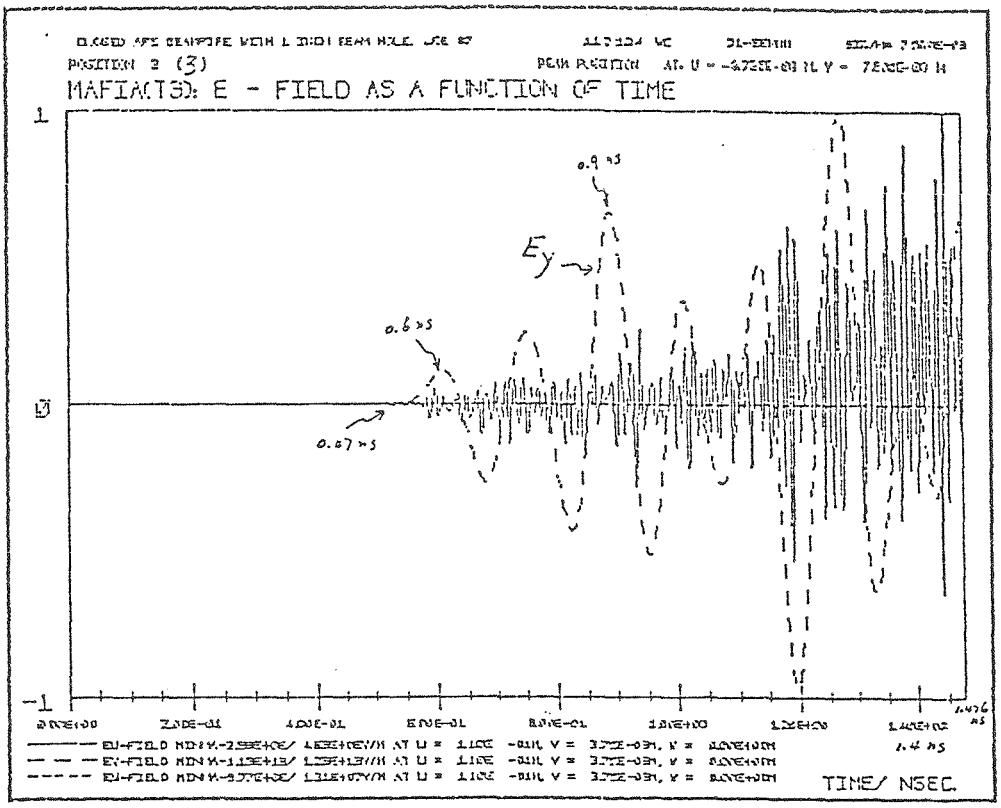

(d)

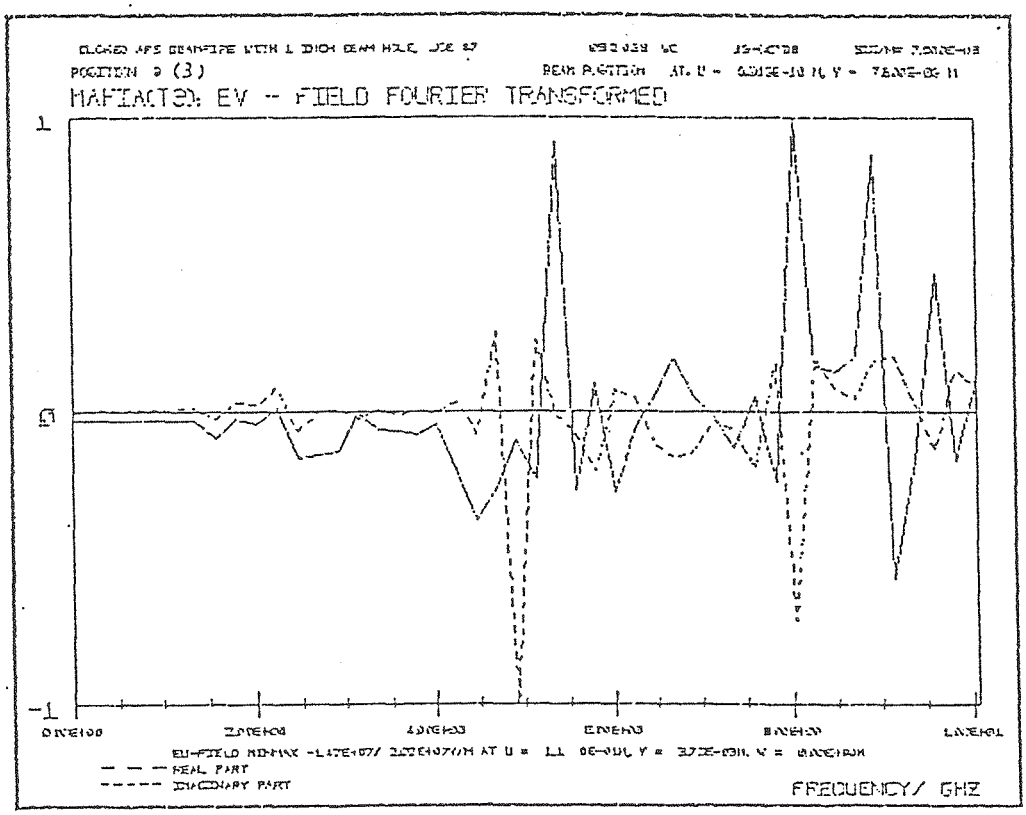

Fig. 4. (c) $\mathbf{E}(t)$ fields in the narrow gap. The major component is E_y of the magnitude 10^{13} V/m. Both E_x and E_z are negligible (six orders of magnitude lower).
(d) The Fourier transform of E_y in the narrow gap. Note that the first peak appears at about 4.6 GHz.

(e)

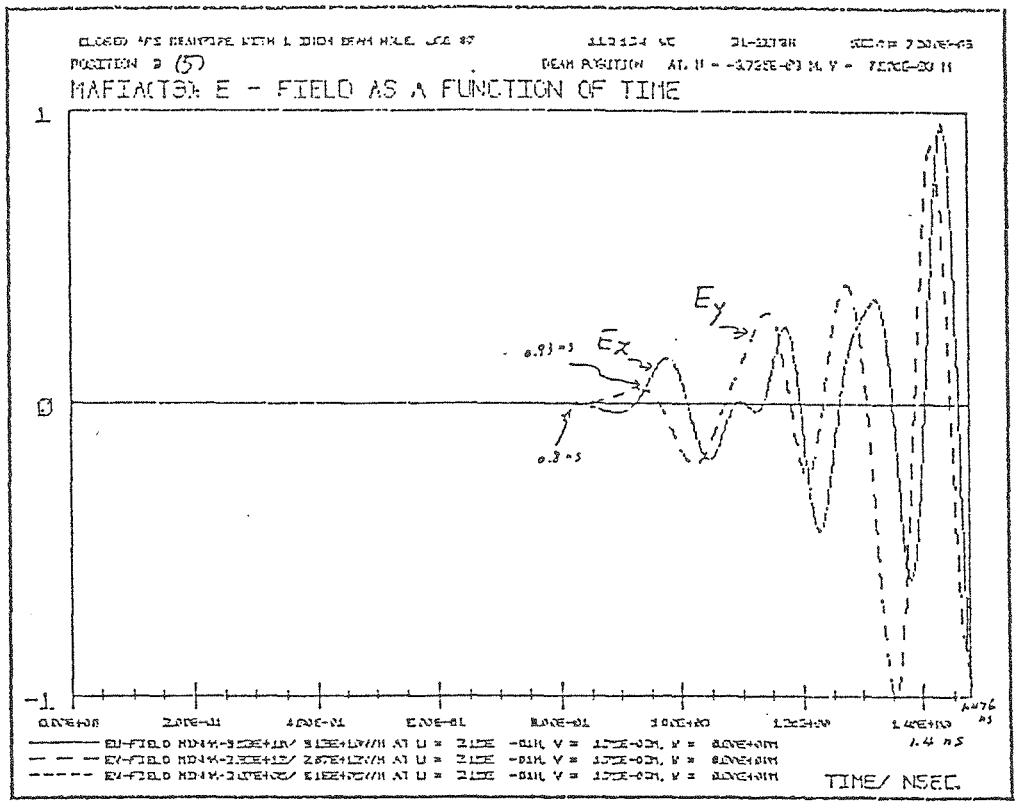

(f)

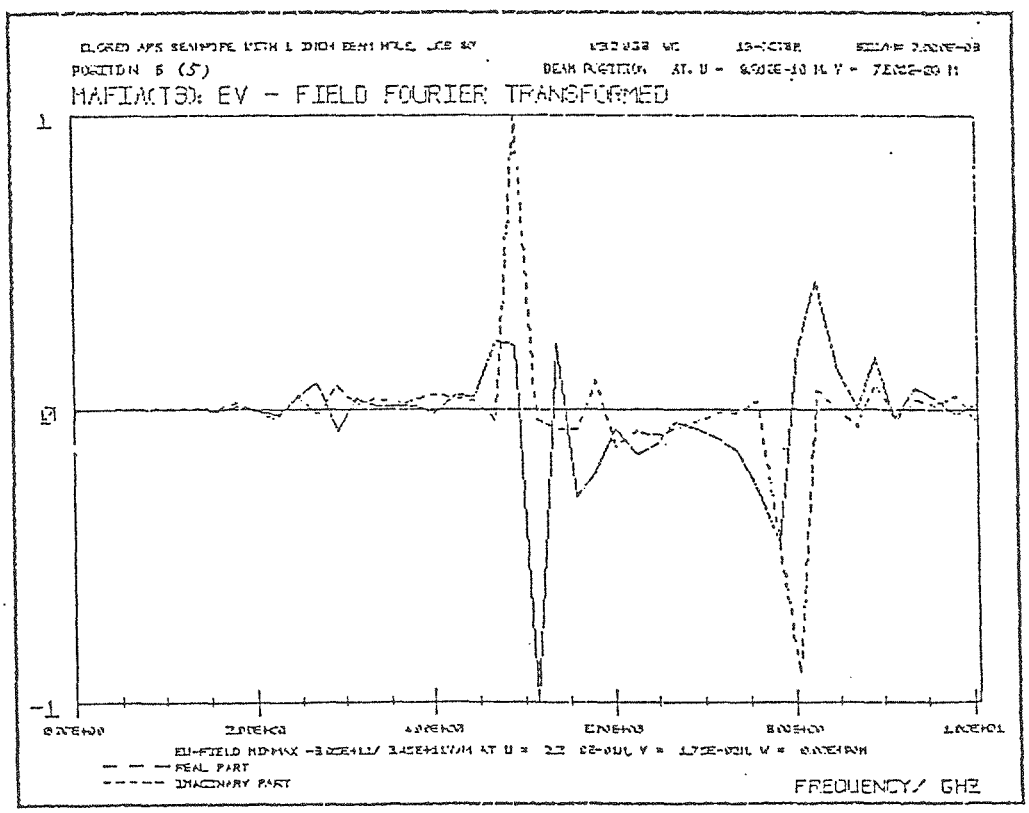

Fig. 4. (e) $\mathbf{E}(t)$ fields in the antechamber. The major component is E_y of the magnitude 10^{13} V/m. E_z is negligible (seven orders of magnitude lower).
(f) The Fourier transform of E_y in the antechamber. Note that the first peak appears at about 4.6 GHz.

(g)

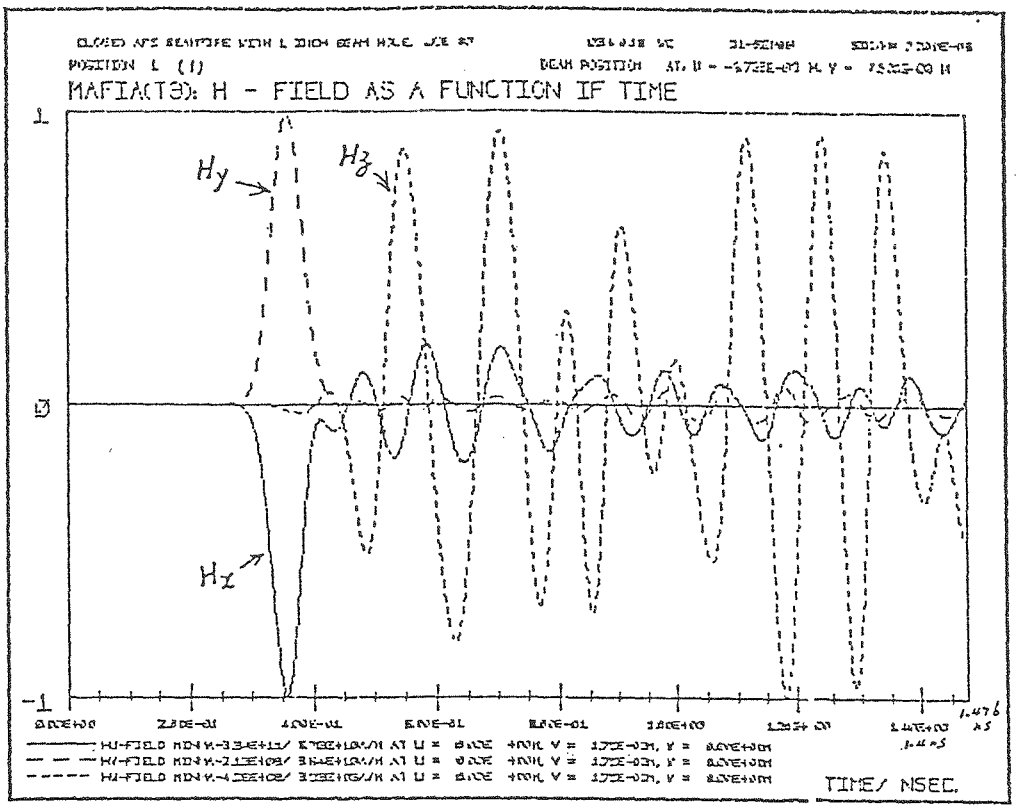

(h)

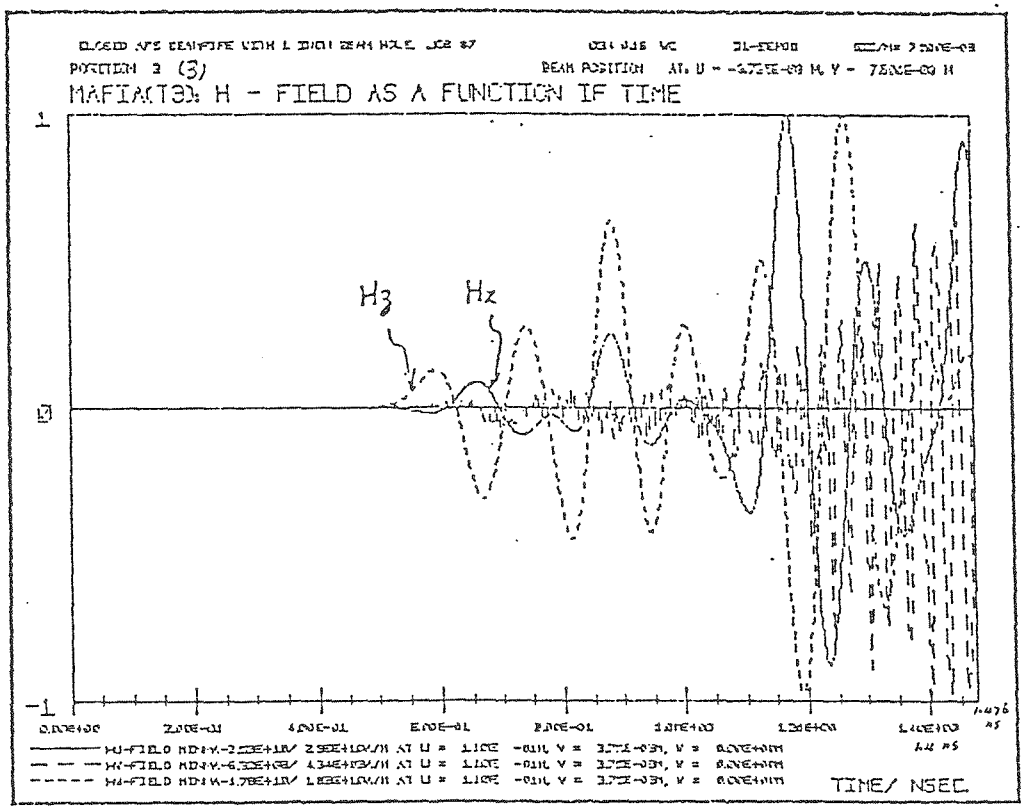

Fig. 4. (g) $\mathbf{H}(t)$ fields in the beam chamber, with magnitude 10^{10} A/m.
(h) $\mathbf{H}(t)$ fields in the narrow gap. The magnitudes of H_x and H_z are 10^{10} A/m, whereas H_y is negligible (seven orders of magnitude lower).

(i)

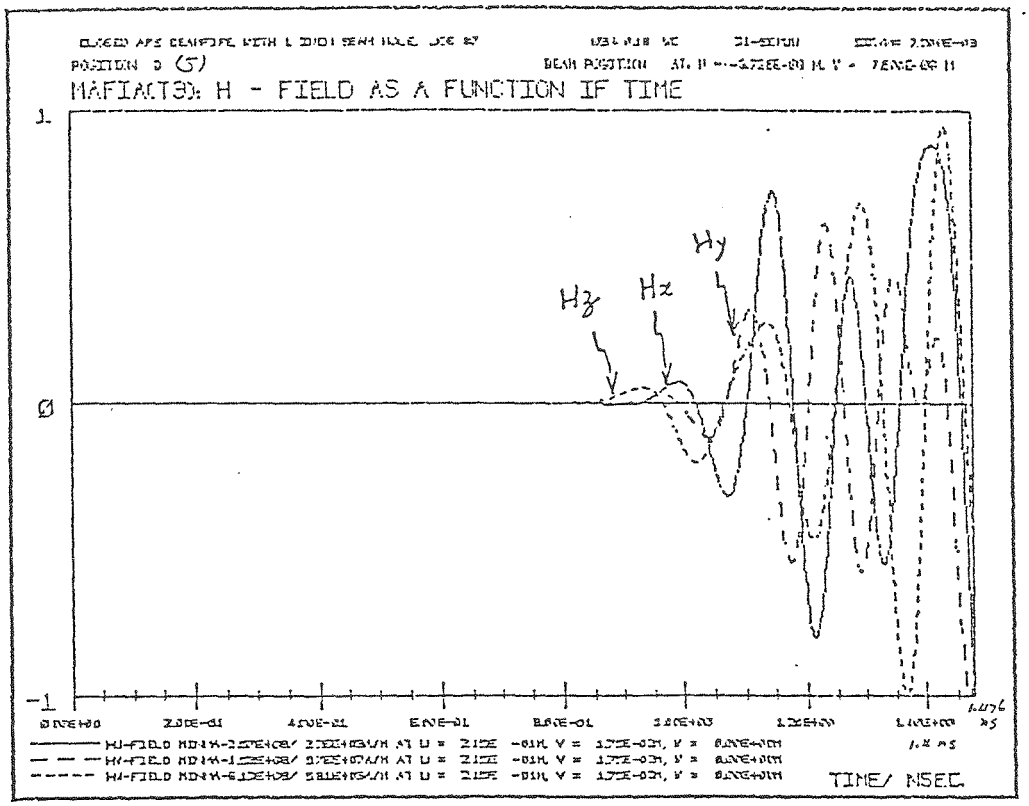

Fig. 4. (i) $\mathbf{H}(t)$ fields in the antechamber, with magnitude 10^9 A/m.

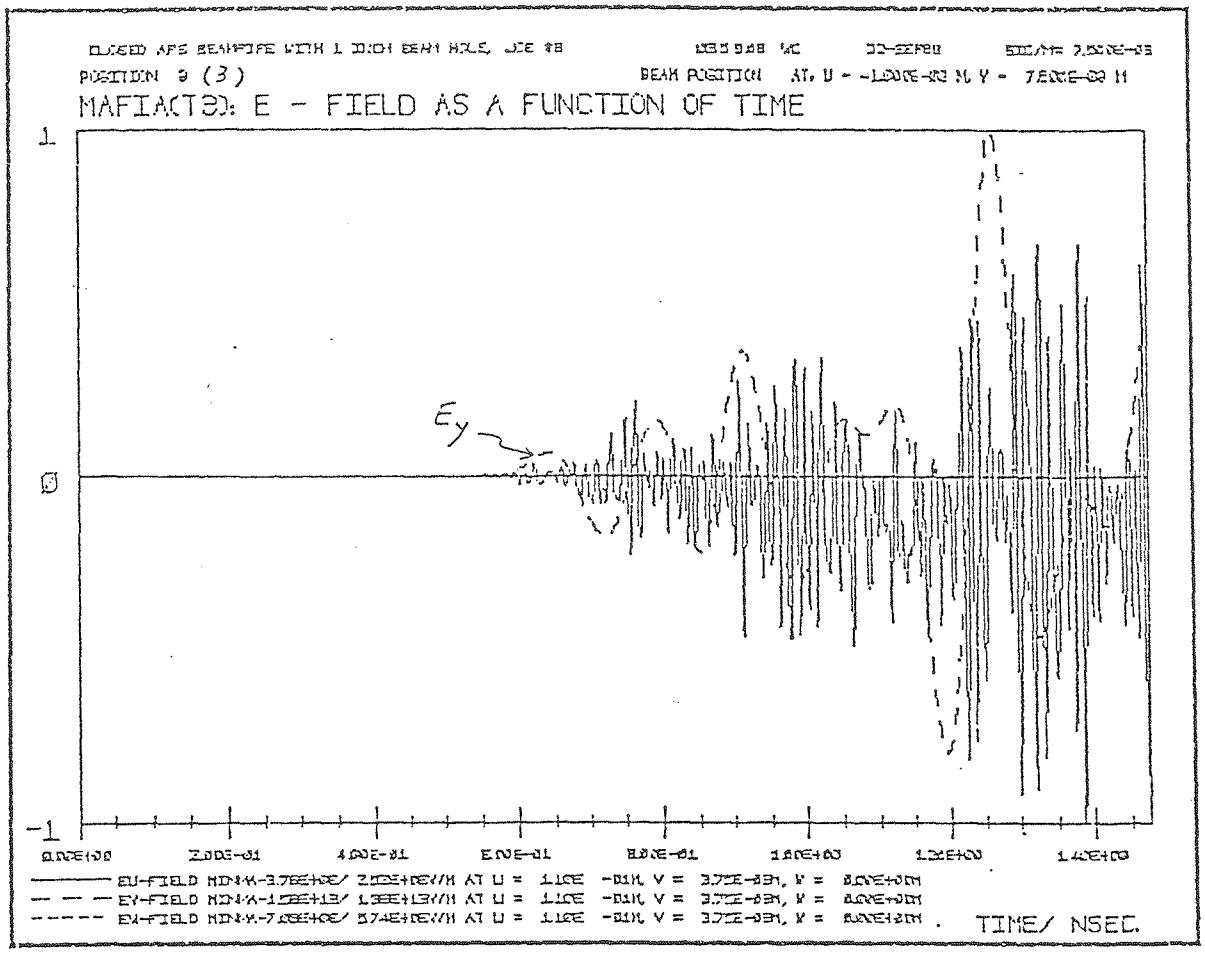

Fig. 5. The $\mathbf{E}(t)$ fields in the gap obtained from run 4 (see text). The E_y component has a magnitude of 10^{13} V/m, while E_x and E_z are negligible.